Coastal upwelling in summer 2000 in the northeastern South China Sea

Dongxiao Wang,[1] Wei Zhuang,[1] Shang-Ping Xie,[2] Jianyu Hu,[3] Yeqiang Shu,[1] and Risheng Wu[4]

Received 1 August 2011; revised 22 December 2011; accepted 10 February 2012; published 5 April 2012.

[1] Using a combination of hydrographic, tide-gauge, near-bottom mooring, and satellite observations; and a numerical circulation model, we investigate the coastal upwelling in the northeastern South China Sea (NSCS) off the coast of Fujian and Guangdong Provinces, China, in the summer of 2000. Subsurface upwelling phenomenon exists mainly near the bottom boundary in the whole region investigated. It is closely related to the coastal sea level fluctuations, which are evidently modulated by both the local wind-forcing and the large-scale circulation. The northeastward interior flow following the bathymetry is accelerated by the drop of coastal sea level and leads to onshore transport and subsequent cooling in the bottom boundary layer (BBL) over the shelf west of Shantou. To the east of Shantou, the near-bottom flow veers more eastward, parallel to the coastline, and transports the nearshore cold water mass farther to the southern Fujian coast. The cross-shelf advected cold water does not always penetrate through the stratification and reach the surface. The local wind exhibits considerable synoptic variability. The decrease in sea surface temperature (SST) is mostly significant near Dongshan-Shantou, intermittent in time and intensifies preferably during weather events that bring southwesterly alongshore wind. To the west a freshwater tongue originating from the Pearl River forms a barrier layer, which results in high surface temperature in the freshwater plume. The observational evidences and modeled results shown in this study provide important information for further understanding the ecological effects associated with the upwelling processes in the NSCS.

Citation: Wang, D., W. Zhuang, S.-P. Xie, J. Hu, Y. Shu, and R. Wu (2012), Coastal upwelling in summer 2000 in the northeastern South China Sea, *J. Geophys. Res.*, *117*, C04009, doi:10.1029/2011JC007465.

1. Introduction

[2] The coastal area off Fujian and Guangdong Provinces (Figure 1) is the confluence region for the Fujian-Zhejiang Coastal Water from the northeast, the South China Sea (SCS) Interior Water from the south, and the Pearl River freshwater plume from the west. The East Asian Monsoon dominates this continental shelf region. In summer, southwesterly winds prevail over most parts of the SCS, but off the coast of South China the climatological winds are southerly, perpendicular to the coast.

[3] Upwelling off the Fujian-Guangdong coast during summer was first reported by *Guan and Chen* [1964] based on the National Comprehensive Oceanographic Survey of China (1958–1960) and subsequently confirmed by hydrographic and satellite investigations [*Chen et al.*, 1982; *Xiao*, 1988; *Li and Li*, 1989; *Hu et al.*, 2001]. *Li et al.* [2000] and *Wang et al.* [2001] showed oceanic fronts near the upwelling region off Fujian and Guangdong from cruise and/or satellite sea surface temperature (SST) observations. Analyses of shipboard measurements in different years indicated considerable variation in the upwelling center along the eastern Guangdong coast during summer [*Zeng*, 1986; *Yu*, 1987; *Han and Ma*, 1988]. *Hong and Li* [1991] suggested that the eastern Guangdong upwelling was part of a basin-scale upwelling in the summer northern SCS. Using satellite SST data, *Tang et al.* [2002] noted that there were several upwelling centers in the vicinity of the Taiwan Strait, one of which took place in southern Fujian near the border with Guangdong. Some recent numerical investigations showed that the eastern Guangdong upwelling was probably driven by local alongshore wind [*Jing et al.*, 2009] and its spatial pattern was modulated by the interactions between coastal currents and local topography [*Gan et al.*, 2009a]. Based on a data assimilation model, *Shu et al.* [2011] noted the existence of upwelling near Shantou during downwelling

[1]State Key Laboratory of Tropical Oceanography, South China Sea Institute of Oceanology, Chinese Academy of Sciences, Guangzhou, China.
[2]International Pacific Research Center and Department of Meteorology, University of Hawai'i at Mānoa, Honolulu, Hawaii, USA.
[3]State Key Laboratory of Marine Environmental Science, Xiamen University, Xiamen, China.
[4]Third Institute of Oceanography, State Oceanic Administration, Xiamen, China.

0148-0227/12/2011JC007465

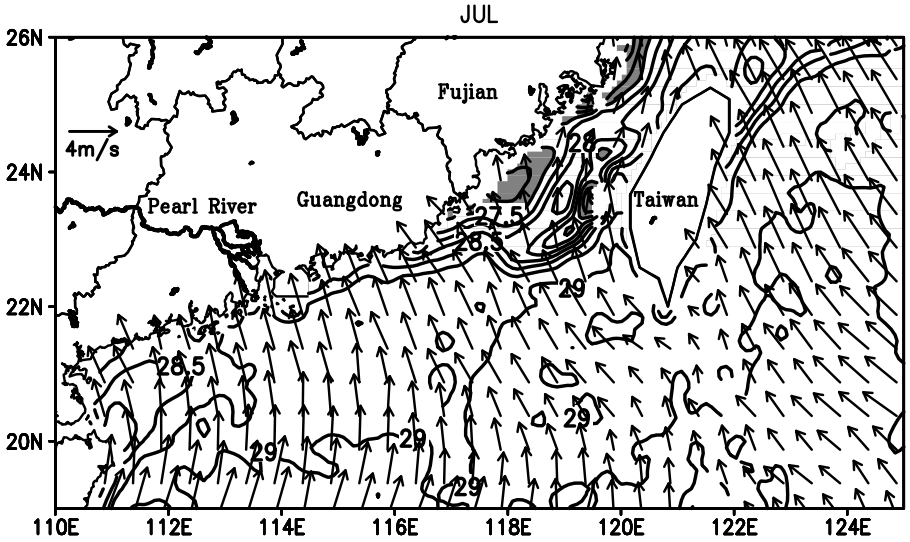

Figure 1. AVHRR SST (contours at 0.25°C intervals) and QuikSCAT wind velocity (m/s) climatology for July of 2000 to 2005, gray shade for SST < 27.5°C.

favorable wind and attributed it to the direction of large-scale current. These studies have improved our understanding of upwelling dynamics in the eastern Guangdong.

[4] The signature of the eastern Guangdong coastal upwelling is evident in the summer SST climatology (Figure 1). An important question remains, however: since monthly mean surface winds in July are nearly perpendicular to the coast, why does coastal upwelling happen at all? Similar wind and SST patterns appear in July of 2000, which as a normal year could be a representative case for the typical upwelling off eastern Guangdong coast. Meanwhile, associated with the surface offshore transport, the vertical structure of onshore return flow, which is critical to understanding the consequences of upwelling, remains poorly understood.

[5] In Figure 1, there exist other two cold zones: one is along the Fujian coast in the northwest of Taiwan Strait, and the other lies in the southeast of Taiwan Bank (mark on Figure 2). These two upwelling zones were also noted in previous studies [*Hu et al.*, 2001; *Tang et al.*, 2002]. But in the present paper, we focus on the upwelling near eastern Guangdong coast and will not investigate the other two zones, which are away from the observational field of our cruise. Based on comprehensive observational results, this study describes the water mass characteristics off eastern Guangdong during the occurrence of coastal upwelling. Then the synergy of observations and model simulations reveals the three-dimensional shelf flow structure related to upwelling processes and illustrates its temporal variations on synoptic timescale. The respective roles of local wind-forcing and basin-scale SCS circulation in the upwelling intensity are further discussed. Below, Section 2 describes the data sets and processing methods; Section 3 presents results, and Section 4 is the summary and discussion.

2. Observations and Model

2.1. Cruise Observational Data

[6] During July 10 to August 2, 2000, a multidisciplinary oceanographic survey from the southern Taiwan Strait to the Pearl River estuary (PRE) was jointly conducted by Xiamen University and the Third Institute of Oceanography, State Ocean Administration of China. The survey consisted of 41 profiles, including three cross-shelf transects, namely P (P1-P9; July 19–21), B (B1-B10; July 30), and A (A13-A1; July 31–August 1) from west to east off Guangdong-Fujian coast, which were sampled by SBE 19 Conductivity–Temperature–Depth (CTD) profiles (Figure 2). Near Dongshan-Shantou coast, there are other 9 profiles, conducted at the shallow region with depth <45 m. To reduce small-scale noise, salinity and temperature profiles in each CTD profile were filtered with a 1-dbar half-width Hanning filter and subsampled at 1 dbar intervals. The station spacing is generally less than 30 km, enabling us to study the cross-shelf structure of temperature and salinity in detail. Measurements of surface variables (temperature, salinity and chlorophyll-*a* concentration) were carried out continuously (10 s sampling interval) along the cruise track (both the dashed and the thick solid line in Figure 2) using an SBE 21 Thermosalinograph equipped with a fluorescence sensor. Data exceeding 3 standard deviations from the mean were removed. Then the quality-controlled data were interpolated onto a 0.1° × 0.1° grid within the observational region by Kriging method. Kriging is a geostatistical gridding method that has proven useful and popular in many fields. This method produces visually appealing maps from irregularly spaced data, compared to other interpolation methods [*Yang et al.*, 2004].

2.2. Mooring Data

[7] In order to monitor the flow on the northeastern South China Sea (NSCS) shelf, 2 moorings were deployed by the South China Sea Institute of Oceanology (SCSIO) at 115.50°E, 21.80°N (M1) and 116.17°E, 21.23°N (M2, see Figure 2). The water depths for M1 and M2 are 100 m and 285 m, respectively. M1 has an AANDERAA RCM-7 current meter at 85 m and M2 contains 2 current meters at 180 m and 265 m. All current meters sampled the velocity and the temperature during 1 June to 29 July 2000 at 10 min

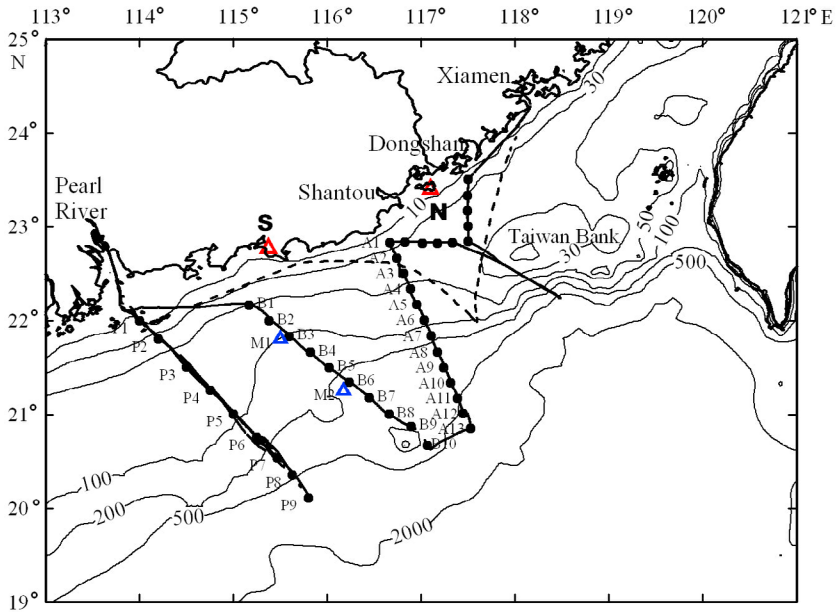

Figure 2. Cruise track (dashed and thick solid lines), CTD stations (dots), and bottom topography (thin contours in meters) of the study area. The dashed line represents the cruise from Xiamen to Pearl River estuary and the thick solid lines represent the return cruise. The moorings M1 and M2 are marked by blue triangles. The tidal gauge stations are marked by red triangles: S (Shanwei) and N (Nanao).

interval. The harmonic analysis [*Pawlowicz et al.*, 2002] was used to remove the tidal currents and preserve the low-frequent residual components. As will be shown in Section 3, the upwelling only occurs in the shelf shallower than 200 m. So M2 does not capture the variability associated with the upwelling processes and this study mainly focuses on the results of M1.

2.3. Tide Gauge Data

[8] Coastal sea level data recorded hourly by tide gauge stations at Nanao (117.10°E, 23.40°N) and Shanwei (115.37°E, 22.77°N) are also analyzed in this study (Figure 2). Nanao is an island east of Shantou within the climatological cold upwelling pool, while Shanwei is to the southwest outside this summer cold center. The static response of the ocean to atmospheric loading was not of interest here and removed by the classical inverted barometer (IB) correction based on the surface air pressure recorded at these two stations. Tides were removed by the harmonic analysis method [*Pawlowicz et al.*, 2002]. The mean sea level during summer 2000 was subtracted from the detided data to obtain sea level anomaly (SLA). Then the SLA data were averaged into daily bins for further analysis.

2.4. Satellite Data

[9] Daily and monthly AVHRR SST data were obtained from NASA Jet Propulsion Laboratory (JPL), with a nominal resolution of 4 km. Because of the high resolution in space and time, the satellite remote sensing SST data have been widely used to detect the hydrographic phenomena around Chinese regional seas [*Zheng and Klemas*, 1982; *Wang et al.*, 2001; *Tang et al.*, 2002; *Xie et al.*, 2003]. The equal-angle best SST data that contain only cloud-masking high quality data are used here [*Vazquez et al.*, 1998]. Atmospheric convection is very active over the SCS in summer, and cloud cover seriously limits AVHRR observations of SST. All data have been calibrated to level 3 using the standard technique with no further corrections. In constructing daily data, both daytime and nighttime SSTs were used to increase the number of data.

[10] The sea surface wind product used in this study was measured by QuikSCAT satellite scatterometer launched in June 1999. Original swath data were mapped to a 0.25° × 0.25° grid by Remote Sensing System (RSS). The grid data for both ascending and descending tracks were averaged to form a daily data set. Daily wind velocity at tidal gauge stations Nanao and Shanwei was estimated from the QuikSCAT data by nearest interpolation. *Xie et al.* [2003] used the QuikSCAT data to study coastal upwelling off South Vietnam, induced by the basin-wide southwesterly summer monsoon in the SCS. The use of high-resolution QuikSCAT data revealed orographic origin of the offshore wind jet east of Ho Chi Minh City, whose curls drove a double-gyre circulation in the SCS.

2.5. Numerical Model

[11] The model used in this study is a three-dimensional primitive equation Princeton Ocean Model (POM) [*Blumberg and Mellor* [1987] applied over the NSCS shelf [*Shu et al.*, 2011]. The model domain extends from 110°E to 120.5°E, and from 18.3°N to 25°N [see *Shu et al.*, 2011, Figure 1]. A curvilinear horizontal grid is utilized with its coordinates (x, y) oriented roughly parallel to alongshore and cross-shore directions, respectively. The horizontal grid spacing is variable, with an average resolution of 5 km. The bottom topography is obtained from ETOPO2 (1/30°) data from the National Geophysical Data Center, which is slightly smoothed to reduce truncation errors. The vertical sigma coordinate has 20 levels and is stretched at upper and bottom levels for more realistic surface and bottom boundary layers. The open

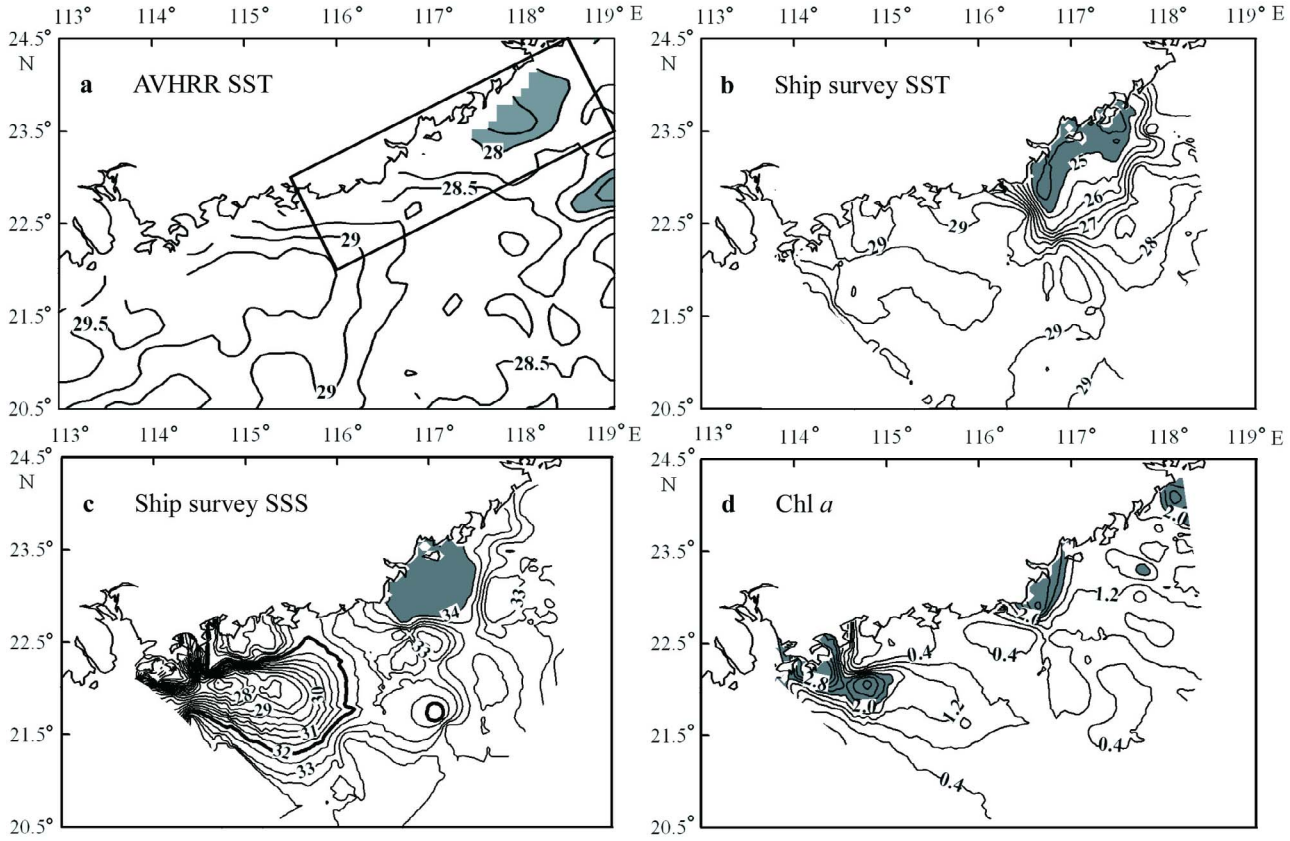

Figure 3. (a) AVHRR sea surface temperature averaged for 10 July−2 August, 2000 (shade < 28°C; contour intervals at 0.25°C). The rectangle represents the coastal low temperature zone. (b) Sea surface temperature (shade < 25°C; contour intervals at 0.5°C). (c) Sea surface salinity (shade > 34; contour intervals at 0.5). The 32 isohaline is marked in bold. (d) Sea surface chlorophyll-*a* (shade > 2.0 mg/m^3; contour intervals at 0.4 mg/m^3). Shipboard observations are used in b–d, with tracks of dashed and thick solid lines in Figure 2.

boundary conditions, applied successfully in the NSCS model by *Shu et al.* [2011], are implemented in this study again.

[12] Initialized at rest with annual mean temperature and salinity fields of the World Ocean Atlas 2001 (WOA01) [*Boyer et al.*, 2005], the model is spun up for 10 years with monthly climatological forcing of wind stress, heat and fresh water fluxes derived from the National Centers for Environmental Prediction/National Center for Atmospheric Research (NCEP/NCAR) reanalysis [*Kalnay et al.*, 1996]. Following the spin-up integration, a simulation from January 1 to August 31, 2000 is conducted with the forcings from observed climatologic monthly Pearl River discharge, daily QuikSCAT sea surface wind and daily NCEP/NCAR air temperature, relative humidity, surface air pressure, cloud cover, precipitation and net shortwave radiation.

3. Results

3.1. Coastal Upwelling Water Mass Characteristics

[13] Figure 3a shows the AVHRR SST distribution averaged during the summer 2000 cruise (10 July to 2 August). The mean QuikSCAT wind velocity field during this period is southwesterly, favorable to the upwelling (not shown). Coastal SST decreases northeastward from the PRE to southern Fujian. There is an SST minimum (<28°C) east of Dongshan Island (∼117.5°E), indicative of upwelling during the period. Figures 3b and 3c display the horizontal distributions of ship survey SST and sea surface salinity (SSS). There is a low temperature and high salinity zone along the Dongshan-Shantou coast. At the center of this upwelling zone, the ship measured SST < 25°C and SSS > 34. Notice that, as the AVHRR map represents the mean SST distribution during the cruise while ship observations are snapshots, ship-observed SST near the Dongshan-Shantou is about 2.5°C lower than the AVHRR SST. The discrepancy between two observations indicates that the upwelling intensity during the cruise is quite variable. As will become clear below, the cruise captures a strong upwelling event in response to southwesterly alongshore winds. To the west, the Pearl River freshwater plume extends eastward (SSS < 33) from the river mouth. This Pearl River diluted water covers the coastal area west of 116°E. Low salinity and low density are the main characteristics of this eastern Guangdong coastal water mass [*Ma et al.*, 1990], which is confined to a shallow surface layer 10 m deep or less. Much greater in volume than that of other rivers in the region, the Pearl River runoff is the main source of freshwater for the coastal water mass and determines the density distribution. In the plume, the satellite and shipboard measurements both detected warm surface water

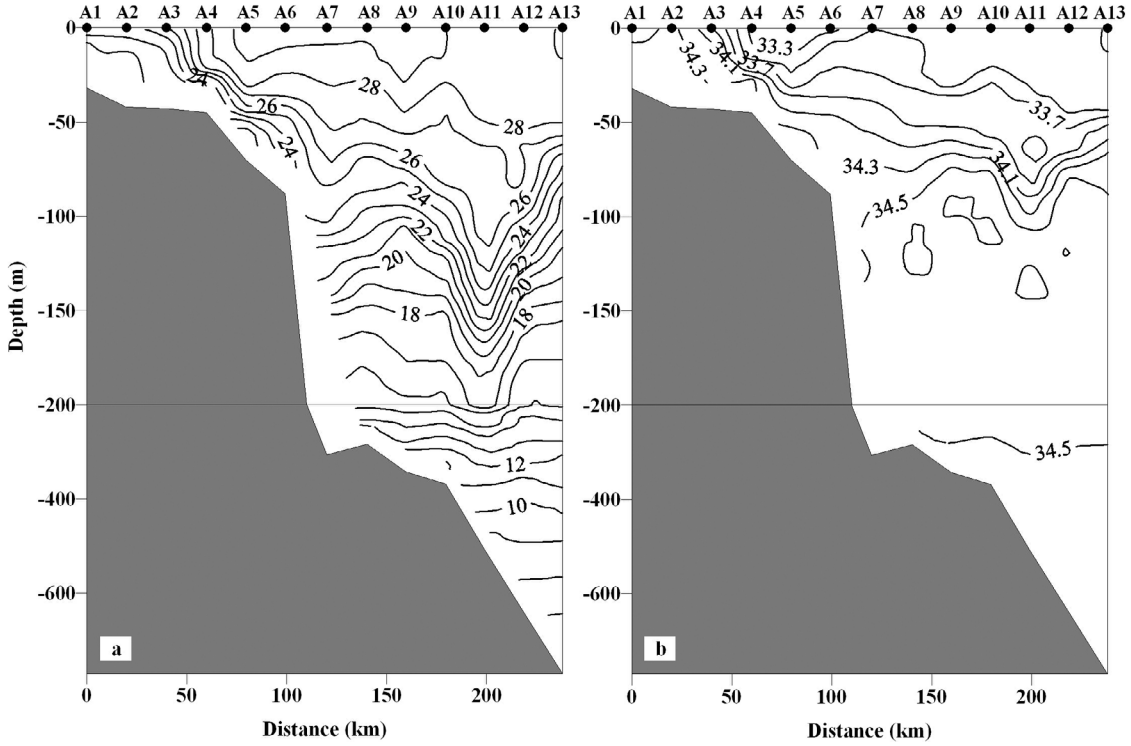

Figure 4. CTD observations at Transect A: (a) temperature (°C, contour interval 1.0) and (b) salinity (contour interval 0.2). Vertical scale changes at 200 m depth.

with temperatures higher than 29.25°C and 29.5°C, respectively. Elevated concentrations of chlorophyll-*a* were observed in both the upwelling zone and the Pearl River plume (Figure 3d). But the nutrient sources of these chlorophyll-*a* maximum zones are different. The former is due to the upwelling, while the latter originates from the Pearl River runoff.

[14] In Transect A (Figure 4), isotherms of values between 23 and 26°C shoal toward the coast and surface. Isohalines between 33.7 and 34.1 show the same onshore shoaling tendency, indicative of thermocline water intrusion onto the continental shelf, i.e., upwelling. This forms a thermohaline front in the upper 20 m between stations A3 and A4. However, the colder (<22°C) and saltier (>34.3) water masses near A1-A2 and at the near-bottom of A5 are not connected with each other. In addition, a warm-core eddy centered at station A11 is also well captured in the offshore region of Transect A. In Transect B (Figure 5), by contrast, the onshore shoaling of isotherms and isohalines is much weaker and confined to near-bottom depth between B1-B2 and around station B4. There is a freshwater lens floating in the upper 10 m between stations B1 and B3, where the local thermocline depth is 40–50 m. A barrier layer between the thermocline and halocline affects SST by reducing the entrainment of cool thermocline water to the surface and results in relatively high SST over the plume (shading area in Figure 5a, also see Figures 3a–3b). Similarly, Transect P (Figure 6) also captures the Pearl River plume between stations P1 and P2. The near-bottom upslope shoaling of isotherms and isohalines between stations P2 and P4 is more pronounced than that in Transect B, but it stops in the subsurface and does not influence the SST. In all these transects, the onshore shoaling phenomena mainly occur over mid- and inner-shelf shallower than 100 m. A recent numerical study by *Gan et al.* [2009a] reproduces the upwelling phenomena in the NSCS and suggests that the subsurface cold water west of Shantou could be advected eastward by costal current and finally outcropped at the lee of the coastline cape near Shantou. However, his process-oriented model is forced by the spatially and temporally uniform wind. Until now, the variability of the upwelling intensity, especially on sub-monthly timescale, and the possible influences of surface wind-forcing and other factors have not been well illustrated. Moreover, the vertical structure of onshore return flow has also not been discussed in previous studies. So these issues will be investigated in the next section.

3.2. Spatiotemporal Variability of Coastal Upwelling

3.2.1. Sea Surface Temperature

[15] The satellite observations from QuikSCAT scatterometer revealed that the surface wind over the eastern Guangdong upwelling region was unsteady and displayed large variations (Figure 7a). During the cruise period (July 10 to August 2), surface wind was generally upwelling-unfavorable until 21 July. After that, upwelling-favorable southwesterly wind prevailed near the eastern Guangdong coast. The SST patterns displayed pronounced contrast between these two periods. During the onshore southeasterly (July 10 to 21), there was no sign of coastal upwelling in the SST data (Figure 7b). During July 22–August 2, by contrast, winds were southwesterly and there was a low SST zone near the coast around 117°E (Figure 7c). Note that the water to the

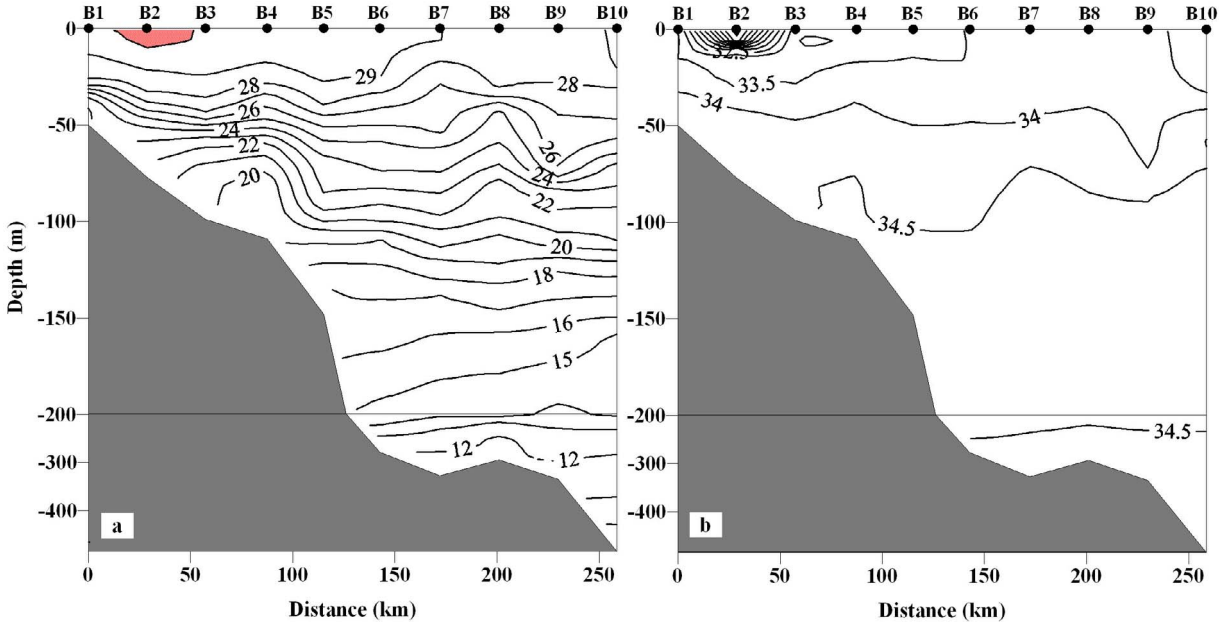

Figure 5. CTD observations at Transect B: (a) temperature (°C, contour interval 1.0) with the region with temperature higher than 29.5°C shaded and (b) salinity (contour interval 0.5). Vertical scale changes at 200 m depth.

southeast of PRE became warmer, suggesting the formation of barrier layer due to strong river runoff and the southeastward Ekman transport on the freshwater plume. The observed SST variations are generally reproduced by the model, wherein the simulated upwelling zone extends relatively more westward than the observation (figures not shown).

[16] We further classified QuikSCAT wind and AVHRR SST during summer of 2000 in two categories: with the positive and negative alongshore wind speed, respectively. Considering the delay of the Ekman response to wind-forcing, we lagged SST by one day in constructing the composites. The impacts of typhoon during July 5–10 (Kai-tak), August 19–23 (Bilis) and August 28–31 (Maria) are not involved into the calculations. The AVHRR SST composite for positive alongshore wind reveals three cold zones during the prevailing of southwesterly (Figure 8a): near the Dongshan-Shantou coast, the northern Fujian coast, and over the Taiwan Bank (an offshore bank roughly

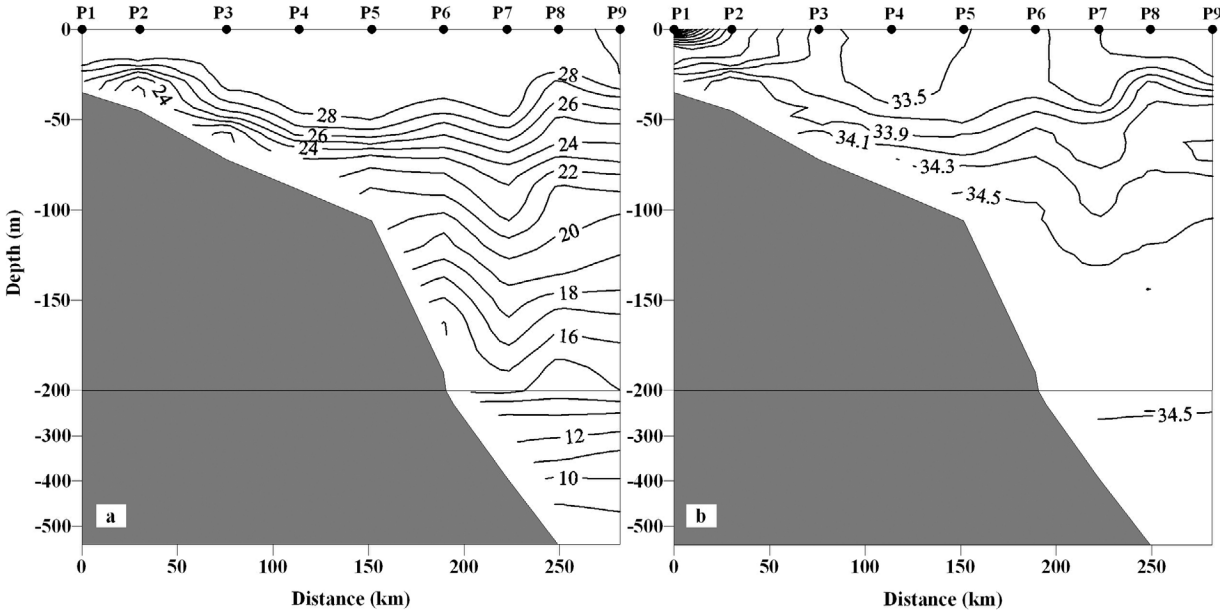

Figure 6. CTD observations at Transect P: (a) temperature (°C, contour interval 1.0) and (b) salinity (contour interval 0.2). Vertical scale changes at 200 m depth.

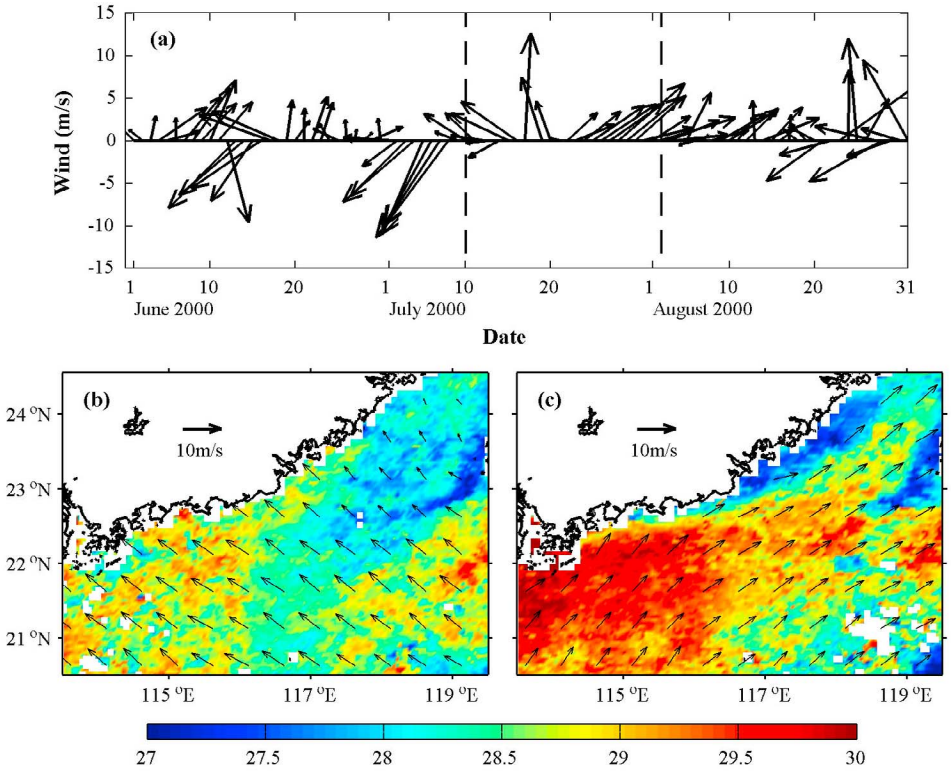

Figure 7. (a) The stick diagram of daily wind velocity averaged over the coastal area (area of the box in Figure 3a) as a function of time during summer 2000. SST and surface wind (b) from July 10 to July 21, 2000 and (c) from July 22 to August 2, 2000.

enclosed by the 40 m bathymetric contour at the south entrance of Taiwan Strait (Figure 2)). In the negative alongshore wind composite, by contrast, the mean surface wind veers to easterly. Sea surface water on the Dongshan-Shantou coast, although still colder than the coastal water to the southwest, is much warmer (Figure 8b) than that in the positive alongshore wind composite. Simulations capture the observed SST difference near Shantou associated with alongshore wind (figures not shown). Thus, upwelling cooling on the Dongshan-Shantou coast is sensitive to variability in alongshore wind during summer 2000, strengthening in response to southwesterly winds.

[17] The moderate cooling on the coast in the negative alongshore wind composite indicates that the coastal current and associated upwelling intensity could be affected not only by surface wind-forcing but also by some other possible

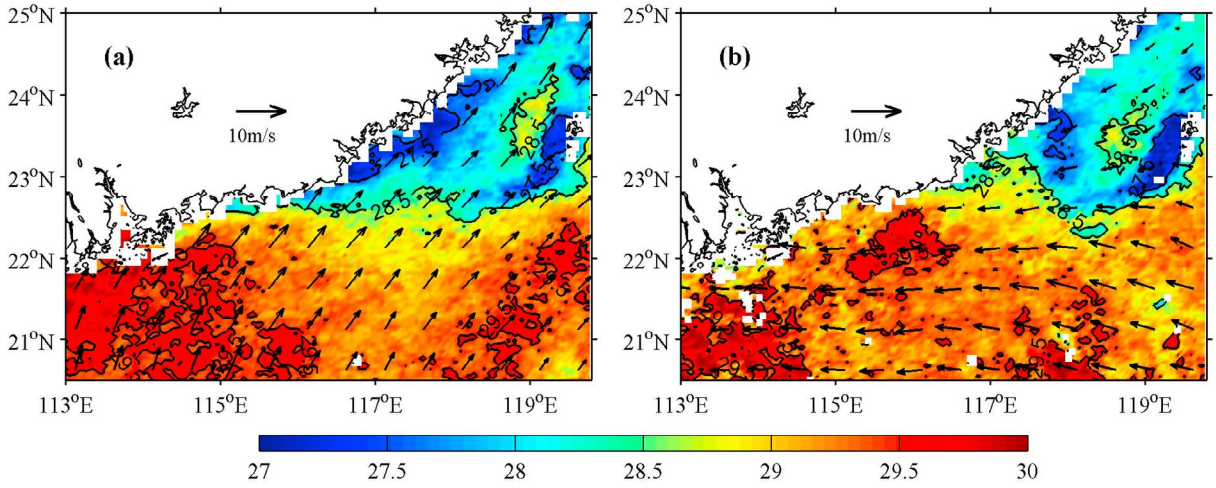

Figure 8. Composite AVHRR SST fields and QuikSCAT wind for (a) positive and (b) negative alongshore wind speed.

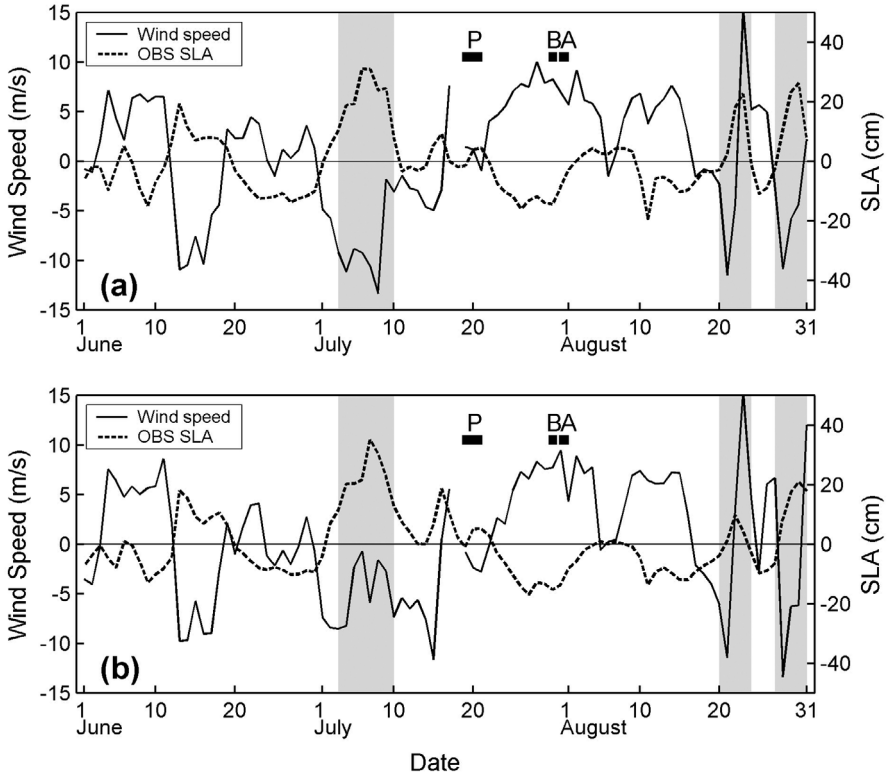

Figure 9. Time series of alongshore wind velocity (solid line) and sea level anomaly (SLA, dashed line) at (a) Nanao and (b) Shanwei stations in summer 2000. The gray shadings indicate the storm surges induced by typhoons. Short horizontal bars mark the sampling periods of Transects P, B and A.

dynamical processes discussed below. AVHRR SST over the Taiwan Bank is significantly low in both composites, suggesting tidal mixing as the cause of this offshore SST minimum. This persistent cooling also indicates that cold water occupies the Taiwan Bank throughout the summer. Its mechanism is beyond the cope of this study.

3.2.2. Sea Level Anomaly

[18] Alongshore wind displays considerable sub-monthly variability (Figure 9), typically between −10 m/s (northeasterly) to 7 m/s (southwesterly), although its summer mean is weak (Figure 1). SLA at Nanao and Shanwei tends to display a quick response to changes in alongshore wind vectors, with sea level dropping in response to upwelling-favorable southwesterly wind and vice versa. As shown in Figure 9, the typical upwelling-favorable wind speed is 5 m/s, leading to a negative SLA of −10 cm. It is noted that SLA shows three pronounced positive peaks, which represent storm surges due to typhoons in the NSCS: Kai-tak (July 5–10), Bilis (August 19–23), and Maria (August 28 - September 1). After removing the impacts of typhoons, the correlation coefficients between SLAs and alongshore wind velocities reach the maxima (−0.57 and −0.59 for Nanao and Shanwei, respectively) when wind leads SLA by one day, in general agreement with the wind-induced upwelling hypothesis [e.g., *Garvine*, 1971]. However, these correlation coefficients are not significant at 90% level of t-test. It indicates that besides local wind-forcing, the coastal SLA in the NSCS could probably be affected by other processes, such as the coastal trapped wave from the north [*Chen and Su*, 1987] or the dynamical adjustment associated with the open ocean circulation [*Wang et al.*, 2010].

[19] To check the possible effect of coastal trapped wave, we compare the coastal SLAs at Nanao and Pingtan (119.78°E, 25.52°N, about 400 km to the northeast of Nanao). The SLAs did not show significant lag correlation (figure not shown), indicating that, during the cruise period, there seemed no coastal trapped wave propagating from the East China Sea to the NSCS. The study of *Chen and Su* [1987] also showed that in summer strong synoptic weather are not as frequent and regular as that in winter, thus the coastal trapped wave characteristics are not as conspicuous.

[20] The samplings of transects P, B and A were not affected by the typhoons. Transect P was taken during a weak southeasterly wind event with nearly zero SLA, while Transects A and B were taken during a long-lived upwelling-favorable wind event of July 22-August 2. All transects show upslope shoaling of isotherms and isohalines above the sea bottom, generally consistent with the relatively low sea level during the sampling periods. But only in Transect A, the thermocline shoaling reaches the sea surface (Figures 3 and 4).

3.2.3. Near Bottom Current and Temperature

[21] The mooring M1 is located very close to the CTD station B3, so the temperature and salinity profiles at B3 could be used to represent the stratification at M1. As shown in Figure 10, the temperature and salinity profiles at B3 indicate that there exists a well-mixed BBL at the depth deeper than 75 m, suggesting that the current meter at 85 m

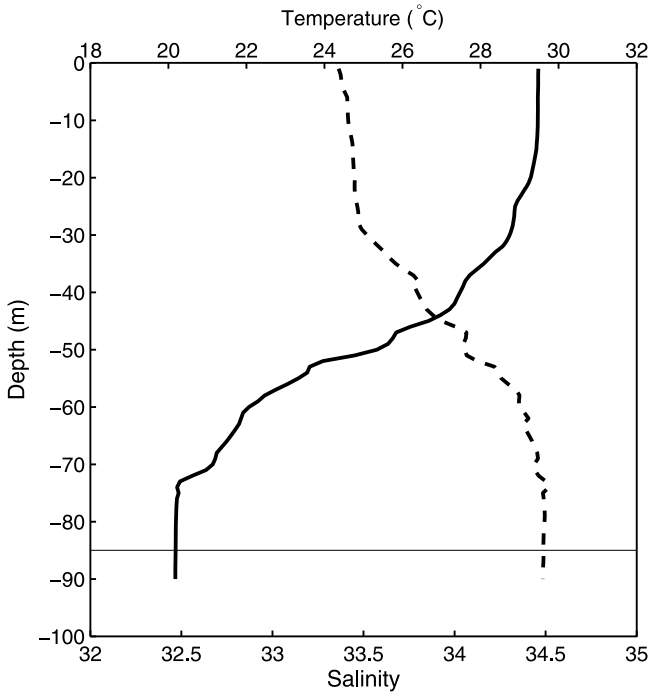

Figure 10. Temperature (thick solid line) and salinity (dashed line) profiles at CTD station B3. The thin solid line indicates the current observing depth at mooring M1.

of M1 generally observes the velocity and temperature within the BBL.

[22] Figure 11a reveals that both the along-shelf and cross-shelf flows at M1 are highly anticorrelated with the sea level fluctuations at Shanwei. The correlation coefficients reach −0.92 and −0.86 for along-shelf and cross-shelf flows respectively, and are both significant at 95% confidence level. To first order the onshore pressure gradient and alongshore current are in geostrophic balance. Thus a drop of SLA on the coast inferring the increase of onshore pressure gradient force will accelerate the alongshore velocity. In the BBL, the same drop in coastal SLA induces an onshore current under the influence of the bottom friction [e.g., *Weatherly and Martin*, 1978; *MacCready and Rhines*, 1993], which our current observations show correspondingly. Figure 11a also shows the cross-shelf velocity and the daily mean temperature tendency (dT/dt) at M1. Here T and dt represent the observed temperature and time interval (1 day), respectively. In response to the cross-shelf transport, temperature tendency in BBL tends to be negative (cooling) during upwelling and positive (warming) during downwelling events. But the correlation between cross-shelf velocity and dT/dt only reaches −0.63, which is below the 95% confidence level, suggesting that alongshore heat transport or diapycnal mixing in the BBL could also pronouncedly affect local temperature variability. The near bottom observations reveal that BBL is an important pathway for the onshore advection of thermocline water near the Guangdong coast.

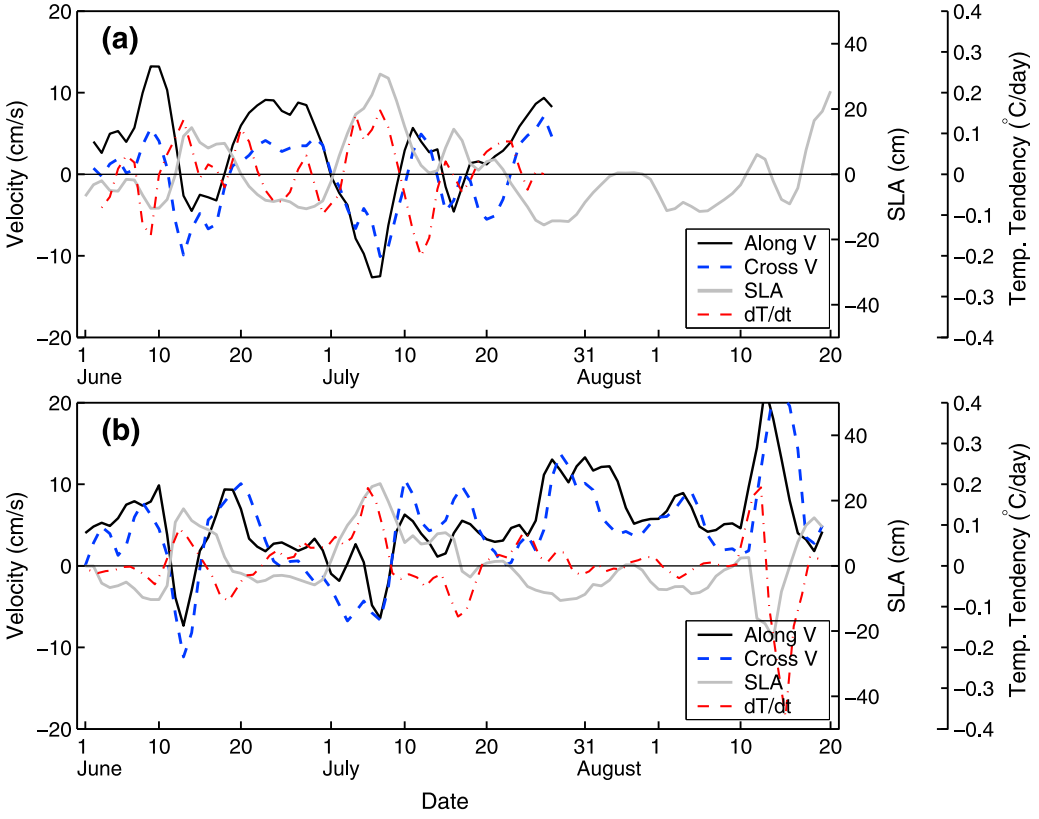

Figure 11. The (a) observed and (b) modeled along-shelf and cross-shelf velocities (cm/s) at M1, daily mean temperature tendency (dT/dt,°C/day) at M1 and the SLA (cm) at Shanwei Station.

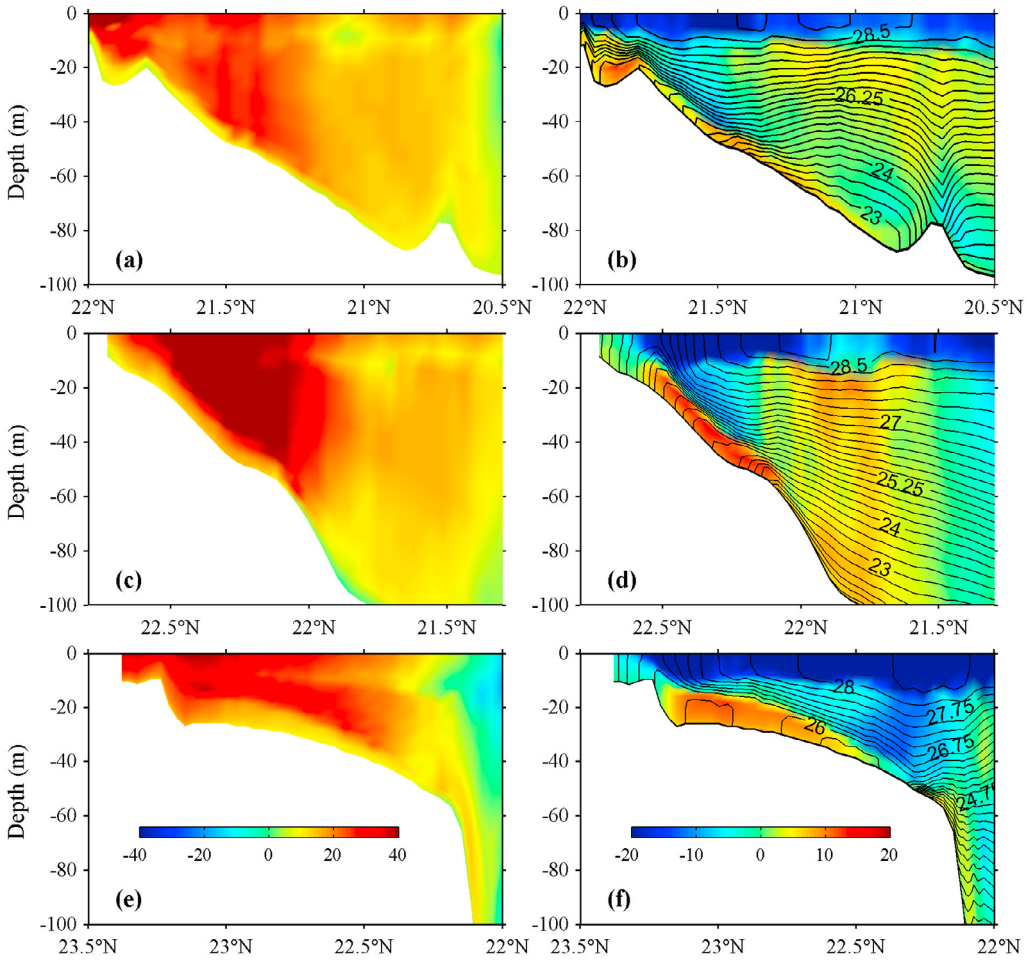

Figure 12. Modeled mean (a) alongshore velocity (cm/s) and (b) cross-shore velocity (shading, cm/s) and temperature (contours at 0.25°C intervals) at Line 1 during 27–31 July 2000. (c) The same as Figure 12a but for Line 2. (d) The same as Figure 12b but for Line 2. (e) The same as Figure 12a but for Line 3. (f) The same as Figure 12b but for Line 3. Lines 1–3 are shown in Figure 13a.

[23] The observed coastal SLA (Figure 11a) is well captured by the model (Figure 11b) with a correlation coefficient of 0.78, above 95% confidence level. The anticorrelation between modeled SLA and near-bottom velocity is not as significant as the observations. The correlation between simulated along-shelf velocity at M1 and SLA at Shanwei reaches −0.74, while the correlation between simulated cross-shelf velocity and SLA is only −0.57, indicating weaker bottom friction and near-bottom current responses (Figure 11b). As shown in Figure 12d, the modeled well-mixed BBL only exists in the area shallower than 60 m off Shanwei. There is not clear BBL at deeper region, due probably to the model's underestimation on the near-bottom mixing. The simulated near-bottom velocities at B1, near 50 m isobath and with a full-developed BBL, are more significantly anticorrelated with the SLA. The correlation coefficients are −0.87 and −0.90 for along-shelf and cross-shelf currents, respectively (figure not shown). As shown in Figure 11b, the near-bottom temperature change at M1 in response to the cross-shelf advection is also reproduced in the model. The correlation between cross-shelf flow and dT/dt is −0.71. Although the temperature changes at one location could not reflect the whole upwelling/downwelling characteristics in the NSCS, the synoptic variations of large-scale SLA and associated near-bottom current in both the observations and simulations demonstrate the intermittent feature of the geostrophic coastal jet and the related upwelling within the BBL.

[24] *Lentz and Chapman* [2004] noted that in coastal upwelling regions around the world, there are substantial differences in the vertical structure of the onshore return flow. They proposed a theory for two-dimensional upwelling that relates the structure of the wind-driven cross-shelf circulation to the Burger number $S = \alpha N/f$, where α is the bottom slope, N is the buoyancy frequency, and f is the Coriolis parameter. For $S \approx 1$ or larger, the bottom stress is small and most of the onshore return flow is in the interior. For $S \ll 1$, the onshore return flow is primarily in the BBL. We have estimated the Burger number over our cruise-survey region shallower than 100 m, where the observed upwelling is the most significant. The bottom slopes are determined with large-scale bathymetry between 30 and 100 m isobaths. The values in Transects A, B and P are all smaller than 1, at S_A = 0.20, S_B = 0.36 and S_P = 0.14, respectively, in accord with large-scale bathymetry $\alpha_B > \alpha_A > \alpha_P$. Referring to *Lentz and Chapman* [2004, Figure 5], our estimates indicate that the onshore transport mainly occurs in the BBL in all three

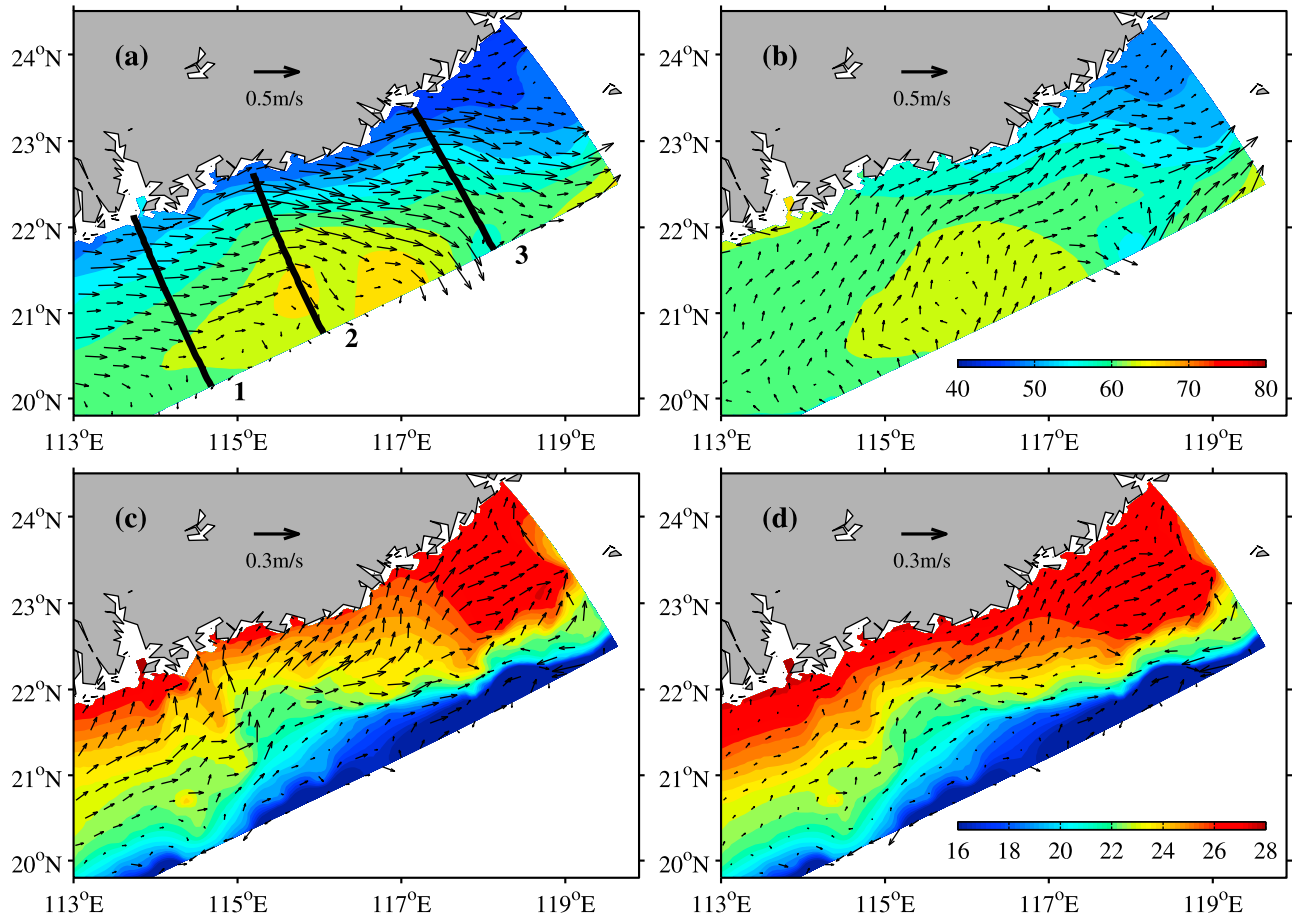

Figure 13. Composite fields of the modeled (a) surface velocity vectors (m/s) and sea level (shading, cm) and (c) bottom velocity vectors (m/s) and bottom temperature (shading, °C) for positive (upwelling favorable) alongshore wind. (b and d) The same as Figures 13a and 13c, respectively, but for negative (upwelling unfavorable) alongshore wind.

transects, among which the interior flow might be relatively more important in Transect B. At M1, basic regime of the Burger number is consistent with the observations and simulations that show the significance of onshore return flow in the BBL in response to coastal sea level fluctuations.

[25] On the other hand, the mooring M2 near station B6 (Figure 2) is too far away offshore and there exists no sign of upwelling (Figure 5). The velocities at M2 are mainly southward (not shown) and do not display variations coherent with coastal SLA.

3.2.4. Modeled Upwelling Flow

[26] The alongshore variations of the three-dimensional velocities and temperature during a typical upwelling event of July 27–31 are shown by 3 vertical transects near PRE, Shanwei and Shantou (Figure 12). The transects are denoted by Lines 1–3 in Figure 13a. The alongshore velocity shows a strong coastal jet over the shelf (Figures 12a, 12c, and 12e). The coastal jet intensifies from south of PRE (Line 1) toward the convex isobaths off Shanwei (Line 2). The intensified alongshore flow, which centers at 50 km offshore, penetrates to the near-bottom and slows down evidently in the BBL by bottom friction (Figure 12c). After passing Shanwei, the alongshore jet continues flowing eastward and weakens again over the widen shelf near Line 3 (Figure 12e).

[27] The cross-shelf currents at these 3 transects display offshore surface Ekman flow driven by the upwelling-favorable wind during July 22–31 (Figures 12b, 12d and 12f). Associated with the deceleration of alongshore velocity, the onshore return flow occurs largely within the BBL of all the 3 transects. The vertical structure of cross-shelf flow is consistent with our estimation based on the Burger number. The strongest onshore current exists between 20 and 60 m isobaths at Transect 2 and evidently advects cold water shoreward. A strong thermal front forms between the interior and the well-mixed BBL (Figure 12d). Similar onshore advection also occurs in the BBL of Transect 3. However, the cold water shoreward of 40 m isobath is not connected with the offshore cold water near the bottom of shelf break region. Similar phenomenon is also observed at Transect A (Figure 4) and simulated by *Gan et al.* [2009a], indicating that the nearshore cold water is advected from upstream by the coastal jet. With the aid of southwesterly wind-forcing, part of the cold water eventually outcrops and results in the coastal SST cooling.

[28] To further illustrate the characteristics of the shelf flow in response to different wind-forcing, we classify the modeled results into the two categories as defined in Figure 8: with the upwelling favorable and unfavorable

winds. The mean sea level during upwelling-favorable wind declines northward from offshore region to the coast (Figure 13a). The lowest sea level locates near Dongshan-Shantou. The surface currents reflect the joint effects of Ekman and geostropic balances. To the west of Line 2, the surface currents flow mostly eastward. After encountering the widen shelf east of Line 2, the currents veer offshore generally following the sea level isolines. Meanwhile, the wind-induced surface Ekman transport orients the current more southeastward. At the same time, the bottom currents over the shelf west of Shantou veer shoreward under the influence of the bottom frictional stress and advect the cold waters from deep region to the inner shelf (Figure 13c). To the east of Shantou, the bottom currents over the shelf mostly flow along the coast and transport the nearshore cold water further toward the northern side of the Taiwan Bank.

[29] In the negative alongshore wind composite, the easterly wind drives onshore Ekman current and significantly weakens the cross-shelf pressure gradient (Figure 13b). The sea level becomes more spatially homogeneous and the weakened shelf currents are mostly northeastward, parallel to the coastline. The mean sea level, which remains lowering toward the coast, is evidently not driven by local easterly wind but affected by external forcing associated with the SCS basin-scale circulation. In response to the deceleration of interior flow, the onshore flow component within the BBL also decreases markedly, resulting in weaker onshore intrusion of cold water and warmer coastal water body (Figure 13d). However, obvious onshore transports by the bottom currents still exist, especially south of Shantou. The model results not only support the observational evidences on the intensification of coastal upwelling by the local southwesterly, but also suggest that even during the upwelling-unfavorable wind, the northeastward interior flow could still be driven by the SCS basin-scale circulation and induce coastal upwelling in the BBL over the NSCS shelf. It is worth noting that in some extreme cases with the alongshore wind ≈ -10 m/s, e.g., June 12–16 and July 3–8 (Figure 9), the coastal sea level rises significantly, causing the reverse of coastal jet and the resultant offshore transport in the BBL (Figure 11).

4. Summary and Discussion

[30] In many upwelling regions, the monthly/seasonal mean winds are favorable for coastal upwelling, e.g., off California, off south Vietnam and east of Hainan within the SCS. The upwelling near the Guangdong-Fujian coast is distinct in that the seasonal mean wind is not upwelling favorable. In the present study, we used in situ observations, tide gauge data, satellite observations and a numerical model to investigate the eastern Guangdong coastal upwelling during the summer of 2000. The results show that although the atmospheric forcing and sea level variability are both large-scale, the SST cooling signature is localized and centered near Dongshan-Shantou coast. *Gan et al.* [2009a] indicated a bathymetric effect: the cold water mass from subsurface upwelling west of 116°E is advected downstream by the coastal jet and eventually outcrops on the widen shelf near Dongshan-Shantou. Our analysis shows the occurrence of this eastward cold advection during the summer of 2000 and further suggests that during this period, the upwelling-induced SST cooling is transient and affected evidently by local synoptic alongshore winds. Therefore, although the monthly mean wind is upwelling unfavorable, the decrease in SST still occurs along the Dongshan-Shantou coast, albeit intermittently.

[31] In the subsurface layer, the upwelling occurs over the entire NSCS shelf. BBL is an important path for the cross-shelf exchanges in the subsurface layer. The modeled results verify that the onshore upwelling flow occurs mainly within the BBL, in accordance with the relevant Burger number estimations proposed by *Lentz and Chapman* [2004]. Both the observation and simulation exhibit the synoptic variations of the near-bottom flows in the BBL which are highly anti-correlated with coastal sea level fluctuations, suggesting that the variability of the along-shelf flow is controlled by the cross-shore pressure gradient force and subsequently results in the cross-shelf flow variations in the BBL due to bottom friction. Similar upwelling processes exist in other upwelling regions, e.g., West Florida shelf [*Weisberg et al.*, 2000, 2001].

[32] The nearshore wind and coastal sea level both exhibit considerable sub-monthly variability. The alongshore wind could significantly modulate the SLA and the flow over the shelf. When the upwelling-favorable southwesterly prevails, the coastal sea level drops conspicuously due to the offshore surface Ekman transport, intensifying the geostrophic alongshore coastal jet and its related onshore bottom Ekman layer transport. However, the wind-forcing is not the only driving factor of coastal upwelling. In the composite for upwelling-unfavorable wind, the mean sea level remains declining toward the coast. The resultant northeastward interior flow, albeit at reduced speed, causes relatively weak onshore advection of cold water in the BBL, suggesting the potential impact of external forcing associated with the SCS basin-scale circulation.

[33] During our study period, the freshwater plume extended eastward from the PRE to 116°E, and formed a local barrier layer, resulting in high SST in the plume. Previous numerical study suggested that the river plume has little effect on the intensity of the upwelling and could only modulate the cross-isobath exchanges within the upper water column [*Gan et al.*, 2009b]. Planned satellite salinity missions, along with SST observations from space, will allow further systematic studies on the effects of Pearl River runoff. Such studies are especially important in light of a possible future decrease in the Pearl River discharge, as the Chinese economy grows and demand for fresh water increases. This is likely to have far-reaching effects on the coastal hydrography and the regional ecosystem.

[34] **Acknowledgments.** We thank Li Li, Jianping Gan, Xiaogang Guo and Xiaopei Lin for their support and helpful comments. This work is supported by the 973 program (2011CB403504), CAS project (KZCX1-YW-12-01, SQ200809), NSFC project (41006011), Joint Funds of the NSFC-GD (U1033003), and Guangdong Natural Science Foundation (S2011010001001).

References

Blumberg, A. F., and G. L. Mellor (1987), A description of a three-dimensional coastal ocean circulation model, in *Three-Dimensional Coastal Ocean Models*, *Coastal Estuarine Sci.*, vol. 4, edited by N. Heaps, pp. 1–16, AGU, Washington, D.C., doi:10.1029/CO004p0001.

Boyer, T., S. Levitus, H. Garcia, R. Locarnini, C. Stephens, and J. Antonov (2005), Objective analyses of annual, seasonal, and monthly temperature

and salinity for the World Ocean on a 0.25° grid, *J. Clim.*, *25*, 931–945, doi:10.1002/joc.1173.

Chen, D., and J. Su (1987), Continental shelf waves along the coasts of China, *Acta Oceanol. Sin.*, *6*(3), 317–334.

Chen, J., Z. Fu, and F. Li (1982), A study on upwelling in Minnan-Taiwan Shoal fishing ground [in Chinese with English abstract], *J. Oceanogr. Taiwan*, *1*(2), 5–13.

Gan, J., A. Cheung, X. Guo, and L. Li (2009a), Intensified upwelling over a widened shelf in the northeastern South China Sea, *J. Geophys. Res.*, *114*, C09019, doi:10.1029/2007JC004660.

Gan, J., L. Li, D. Wang, and X. Guo (2009b), Interaction of a river plume with coastal upwelling in the northeastern South China Sea, *Cont. Shelf Res.*, *29*, 728–740, doi:10.1016/j.csr.2008.12.002.

Garvine, R. W. (1971), A simple model of coastal upwelling dynamics, *J. Phys. Oceanogr.*, *1*, 169–179, doi:10.1175/1520-0485(1971)001<0169:>ASMOCU>2.0.CO;2.

Guan, B. X., and S. J. Chen (1964), The current systems in the near-sea area of China seas [in Chinese with English abstract], technical report, 85 pp., Inst. of Oceanol. Chin. Acad. of Sci., Qingdao, China.

Han, W., and K. Ma (1988), A study of eastern Guangdong coastal upwelling [in Chinese with English abstract], *Acta Oceanol. Sin.*, *10*(1), 52–60.

Hong, Q., and L. Li (1991), A study of upwelling over continental shelf off eastern Guangdong [in Chinese with English abstract], *J. Oceanogr. Taiwan*, *10*(3), 271–277.

Hu, J., H. Kawamura, H. Hong, M. Suetsugu, and M. Lin (2001), Hydrographic and satellite observations of summertime upwelling in the Taiwan Strait: A preliminary description, *Terr. Atmos. Oceanic Sci.*, *12*(2), 415–430.

Jing Z., Y. Qi, Z. Hua, and H. Zhang (2009), Numerical study on the summer upwelling system in the northern continental shelf of the South China Sea, *Cont. Shelf Res.*, *29*, 467–478, doi:10.1016/ j.csr.2008.11.008.

Kalnay, E., et al. (1996), The NCEP/NCAR 40-year reanalysis project, *Bull. Am. Meteorol. Soc.*, *77*, 437–471, doi:10.1175/1520-0477(1996)077<0437:TNYRP>2.0.CO;2.

Lentz, S. J., and D. C. Chapman (2004), The importance of nonlinear cross-shelf momentum flux during wind-driven coastal upwelling, *J. Phys. Oceanogr.*, *34*, 2444–2457, doi:10.1175/JPO2644.1.

Li, L., and D. Li (1989), Summer hydrographic features of channel west of Taiwan Shoal and the coastal upwelling [in Chinese with English abstract], *J. Oceanogr. Taiwan*, *8*(4), 353–359.

Li, L., X. Guo, and R. Wu (2000), Oceanic fronts in southern Taiwan Strait [in Chinese with English abstract], *J. Oceanogr. Taiwan Strait*, *19*(2), 147–156.

Ma, Y., S. Xu, and H. Zhong (1990), *Report on Decadal Hydrographic Investigations in the Sea Area Adjacent to the Shelf of the Northern South China Sea [in Chinese]*, 254 pp., China Ocean, Beijing.

MacCready, P., and P. B. Rhines (1993), Slippery bottom boundary layers on a slope, *J. Phys. Oceanogr.*, *23*, 5–22, doi:10.1175/1520-0485(1993)023<0005:SBBLOA>2.0.CO;2.

Pawlowicz, R., B. Beardsley, and S. Lentz (2002), Classical tidal harmonic analysis including error estimates in MATLAB using T_TIDE, *Comput. Geosci.*, *28*, 929–937, doi:10.1016/S0098-3004(02)00013-4.

Shu, Y. Q., D. X. Wang, J. Zhu, and S. Q. Peng (2011), The 4-D structure of upwelling and Pearl River plume in the northern South China Sea during summer 2008 revealed by a data assimilation model, *Ocean Modell.*, *36*(3–4), 228–241, doi:10.1016/j.ocemod.2011.01.002.

Tang, D., D. R. Kester, I.-H. Ni, H. Kawamura, and H. Hong (2002), Upwelling in the Taiwan Strait during the summer monsoon detected by satellite and shipboard measurements, *Remote Sens. Environ.*, *83*, 457–471, doi:10.1016/S0034-4257(02)00062-7.

Vazquez, J., P. Kelly, and K. Kilpatrick (1998), NOAA/NASA AVHRR Oceans Pathfinder sea surface temperature data set user's reference manual version 4.0, *JPL Publ.*, *D-14070*.

Wang, D., Y. Liu, Y. Qi, and P. Shi (2001), Seasonal variability of thermal fronts in the northern South China Sea from satellite data, *Geophys. Res. Lett.*, *28*, 3963–3966, doi:10.1029/2001GL013306.

Wang, D., B. Hong, J. Gan, and H. Xu (2010), Numerical investigation on propulsion of the counter-wind current in the northern South China Sea in winter, *Deep Sea Res., Part I*, *57*(10), 1206–1221, doi:10.1016/j.dsr.2010.06.007.

Weatherly, G. L., and P. J. Martin (1978), On the structure and dynamics of the oceanic bottom boundary layer, *J. Phys. Oceanogr.*, *8*, 557–570, doi:10.1175/1520-0485(1978)008<0557:OTSADO>2.0.CO;2.

Weisberg, R. H., B. D. Black, and Z. Li (2000), An upwelling case study on Florida's west coast, *J. Geophys. Res.*, *105*, 11,459–11,469, doi:10.1029/2000JC900006.

Weisberg, R. H., Z. Li, and F. E. Muller-Karger (2001), West Florida shelf response to local wind forcing: April 1998, *J. Geophys. Res.*, *106*, 31,239–31,262, doi:10.1029/2000JC000529.

Xiao, H. (1988), Studies of coastal upwelling in western Taiwan Strait [in Chinese with English abstract], *J. Oceanogr. Taiwan*, *7*(2), 135–142.

Xie, S.-P., Q. Xie, D. Wang, and W. T. Liu (2003), Summer upwelling in the South China Sea and its role in regional climate variations, *J. Geophys. Res.*, *108*(C8), 3261, doi:10.1029/2003JC001867.

Yang, C., S. Kao, F. Lee, and P. Hung (2004), Twelve different interpolation methods: A case study of Surfer 8.0, paper presented at Geo-Imagery Bridging Continents, Int. Soc. for Photogramm. and Remote Sens., Istanbul, Turkey, 12–23 July.

Yu, W. (1987), A preliminary approach of the upwelling for the northern South China Sea [in Chinese], *Mar. Sci.*, *6*, 7–10.

Zeng, L. (1986), A preliminary analysis of indicators of offshore upwelling off eastern Guangdong [in Chinese with English abstract], *J. Trop. Oceanol.*, *5*(1), 68–73.

Zheng, Q., and V. Klemas (1982), Determination of winter temperature patterns, fronts, surface currents in the Yellow Sea and East China Sea from satellite imagery, *Remote Sens. Environ.*, *12*, 201–218, doi:10.1016/0034-4257(82)90053-0.

J. Hu, State Key Laboratory of Marine Environmental Science, Xiamen University, Xiamen 361005, China.

Y. Shu, D. Wang, and W. Zhuang, State Key Laboratory of Tropical Oceanography, South China Sea Institute of Oceanology, Chinese Academy of Sciences, 164 West Xingang Rd., Guangzhou 510301, China. (dxwang@scsio.ac.cn)

R. Wu, Third Institute of Oceanography, State Oceanic Administration, Xiamen 361005, China.

S.-P. Xie, International Pacific Research Center and Department of Meteorology, University of Hawai'i at Mānoa, Honolulu, HI 96822, USA.